PCCP

Accepted Manuscript

ROYAL SOCIETY OF CHEMISTRY

www.rsc.org/pccp

Journal Name

RSCPublishing

ARTICLE

Exploring the structure-aromaticity relationships in Hückel and Möbius N-fused pentaphyrins using DFT

Cite this: DOI: 10.1039/x0xx00000x

Received 00th January 2012,
Accepted 00th January 2012

DOI: 10.1039/x0xx00000x

www.rsc.org/

M. Alonso,*[a] P. Geerlings[a] and F. De Proft[a]

N-fused pentaphyrins (NFP) are the stable forms of fully *meso*-aryl pentaphyrins(1.1.1.1.1). In order to determine the optimum conditions for *viable* Möbius topologies of these porphyrinoids, the conformational preferences, Hückel-Möbius interconversion pathways and aromaticity of [22] and [24]NFP have been investigated using density functional theory calculations. The conformation of the macrocycle is shown to be strongly dependent on the oxidation state and the macrocyclic aromaticity. [22]NFP prefer a highly aromatic and relatively strain-free Hückel conformation. However, antiaromatic Hückel and weakly aromatic Möbius conformers coexist in dynamic equilibrium in the [24]NFP. The Hückel-Möbius aromaticity switch requires very low activation energy barriers (E_a = 3-4 kcal mol^{-1}). Interestingly, the balance between Möbius and Hückel conformations in [24]NFP can be controlled by *meso*-substituents. The structure-property relationships between the molecular conformation, number of π electrons and aromaticity have been established in our study using energetic, magnetic, structural, and reactivity descriptors of aromaticity. Although the Möbius topology is indeed accessible for [24]NFP**,** it does not exhibit a distinct macrocyclic aromaticity mainly due to the large dihedral angles around the molecular twist. Regarding to the computational methodology, B3LYP and M06 show the best overall performance for describing the experimental geometries of NFP and, importantly, our computational results support the experimental evidence available for N-fused pentaphyrins.

Introduction

Expanded porphyrins, the higher homologues of porphyrins, have attracted considerable attention in the last decade due to their exceptional optical, electrochemical and coordination properties.[1,2] The rich chemistry of expanded porphyrins has led to a diverse family of structures with applications as ion sensors,[3] near-infrared dyes,[4] two-photon absorption materials[5] and nonlinear optical materials.[6] Moreover, expanded porphyrins have some definite advantages in the formation of Möbius aromatic molecules such as (*i*) overall conformational flexibility, (*ii*) multiple oxidation states which can be easily interconverted by two-electron redox reactions, (*iii*) ability to invert, or "flip out", the pyrrolic subunits under certain conditions and (*iv*) possibility of "locking in" Möbius conformations through metalation by the formation of both N-metal and C-metal bonds.[1]

These large macrocycles are the most appropriate molecular systems to test the practical limits of the Hückel rule for aromaticity and antiaromaticity since a set of congeners with [4*n*]/[4*n*+2] π electrons can be synthetized readily.[7] Hückel's rule has long been the basis of our understanding of aromaticity, provided that a conjugated electronic circuit is lying on a normal two-sided plane. Within this two-sided planar topology, an aromatic compound is a cyclic molecular structure stabilized by the delocalization of [4*n*+2] π electrons, while cyclic compounds with [4*n*] π electrons are antiaromatic and unstable. On the other hand, the concept of Möbius aromaticity predicts that the Hückel rule should be reversed for those π systems that lie on a singly twisted Möbius topology.[8] Nevertheless, the realization of Möbius aromatic molecules was quite difficult owing to the structural requirements of implementing a smooth conjugated π network and a twisted conformation within a single molecule.[9]

The conformational flexibility of expanded porphyrins allows them to achieve Hückel and Möbius topologies with distinct aromaticity and photophysical properties.[10,11] Experimental studies have shown that there is a close relationship between the molecular topology, aromaticity and nonlinear optical properties.[12] In general, aromatic expanded porphyrins, both Hückel and Möbius, exhibit larger two-photon absorption (TPA) cross-section values than the antiaromatic ones. In addition,

within a closely related series of compounds, it was found that compounds with greater aromatic character give rise to higher TPA cross-section values.[13] Therefore, aromaticity provides a simple measure of the photophysical properties of the system.

Nevertheless, the quantification of aromaticity in expanded porphyrins is difficult. Nowadays, the annulene model is widely used to predict the aromaticity of porphyrinoids.[14] According to this model, the ring system of a porphyrinoid is treated as a bridged heteroannulene, so aromaticity can be predicted in a qualitative way by formally applying the [4*n*+2] Hückel rule to the annulene substructure.[15] However, these macrocycles sustain multiple conjugation pathways and, in principle, Hückel´s rule should not be applied to polycyclic π-systems. In addition, aromaticity is currently described as a multidimensional phenomenon, implying that the aromatic character cannot be quantified using a single numerical criterion.[16,17] Very recently, we proposed a set of aromaticity descriptors to quantify the aromaticity of Möbius and Hückel expanded porphyrins based on energetic, magnetic, structural, and reactivity criteria.[18] The isomerization method was proven to be an effective method for evaluating aromatic stabilization energies (ISE),[19] magnetic susceptibility exaltation[20] (Λ) and relative hardness[21] ($\Delta\eta$) of expanded porphyrins. It was the first time that these popular aromaticity indices were applied to porphyrinoids. The aromaticity analysis was complemented with the calculation of the structural descriptor HOMA[22] and several NICS-based magnetic indices.[23] Herein, these aromaticity indices are applied to quantify the aromaticity of N-fused pentaphyrins (NFP) in order to characterize the minimum size of pyrrolic macrocycles that can achieve Möbius aromaticity (Scheme 1). Previously, we found that Möbius topologies are indeed accessible for [*4n*] π expanded porphyrins, although fully aromatic Möbius structures are only achievable by protonated [32]heptaphyrin[24] and [28]hexaphyrin.[18]

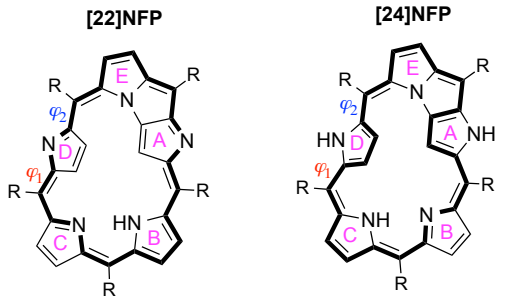

Scheme 1. Molecular structures of the N-fused [22] and [24]pentaphyrins. The classical conjugation pathway is depicted with bold bonds.

Regarding to the regular pentaphyrins(1.1.1.1.1), we found that the N-fusion reaction is thermodynamically spontaneous with five *meso*-substituents, driven by the release of ring strain.[25] Accordingly, N-fused pentaphyrins (NFP) are the stable forms of fully *meso*-aryl pentaphyrins(1.1.1.1.1).[26] An attractive feature of N-fused pentaphyrins is their ability to adopt two stable oxidation states, corresponding to a 22π- and 24π-electronic states ([22]NFP and [24]NFP), which can be easily interconverted by two-electron redox reactions.[27] Interestingly, [24]NFP provided the smallest Möbius aromatic system with a distinct diatropic current upon Rh(I) metalation[28] and a triply fused conformation upon phosphorus insertion.[29]

As a continuation of our research toward the design of Möbius aromatic expanded porphyrins using computational chemistry, we examined the conformational preferences, interconversion pathways and aromaticity of N-fused [22] and [24]pentaphyrins (Scheme 1). Herein, the viability of Möbius topologies in N-fused pentaphyrins is analysed and the structure-property relationships between the molecular conformation, aromaticity and number of π electrons is established. It is shown that the conformation of the N-fused macrocycle strongly depends on the oxidation state and *meso*-substituents. In addition, the performance of several exchange-correlation density functionals (B3LYP, B3LYP-D, and M06) on the geometries and relative conformational energies has been assessed from comparison with experiment.

Computational Details

All calculations have been performed with the Gaussian 09 program[30] using the three parameter B3LYP functional[31] with the 6-31G(d,p) basis set.[32] In previous works, B3LYP was concluded to show the best overall performance for describing geometries and thermochemistry of hexaphyrins[18] and heptaphyrins.[24] The use of larger basis set like 6-311+G(d,p) resulted in very small changes in the relative energies and activation barriers.[18] In any case, the performance of the empirical dispersion correction[33] (DFT-D) and the M06 functional[34] on the geometries and energies of several substituted N-fused pentaphyrins has also been assessed.

Relaxed potential energy (PES) surfaces for **1**-**2** were performed at B3LYP/6-31G(d,p) level of theory, in order to locate the most stable conformations and transition states. Two internal dihedral angles, centered on carbon-carbon bonds (φ_1 or φ_2 in Scheme 1), were chosen for constructing the 3D PES. All local minima and transition states were further optimized without any geometrical restriction and characterized by frequency calculations. For the transition states, only one imaginary frequency was found corresponding to the rotation of these dihedral angles. The geometries of Hückel and Möbius conformers of N-fused pentaphyrins **3**-**10** were fully optimized and characterized by harmonic vibrational frequency computations.

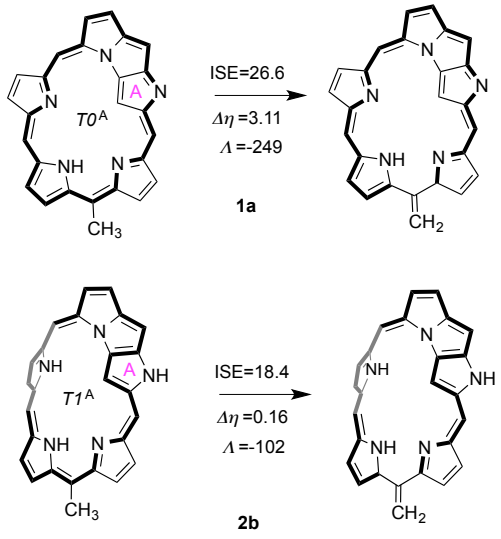

Scheme 2. Reactions used to evaluate the isomerization stabilization energy (ISE), the magnetic susceptibility exaltation (Λ) and the relative hardness ($\Delta\eta$) of N-fused pentaphyrins. ISE and $\Delta\eta$ are given in kcal mol^{-1} and Λ in ppm cgs.

Journal Name RSCPublishing

ARTICLE

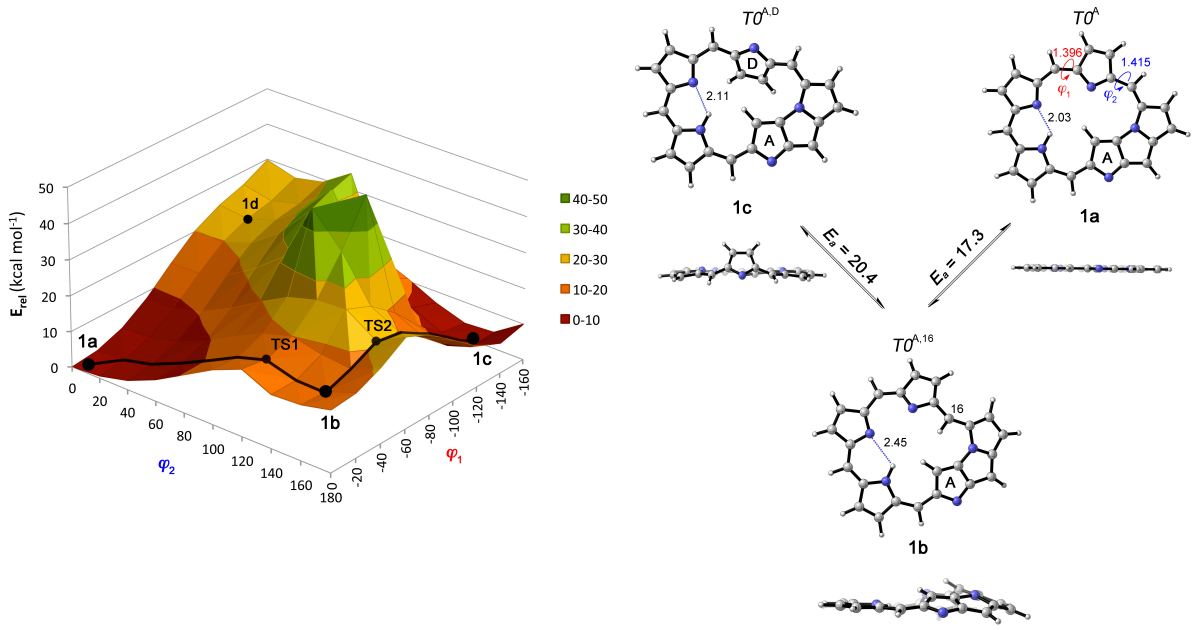

Figure 1. B3LYP/6-31G(d,p) relaxed energy potential surface for the [22]NFP **1** obtained by rotating the dihedral angles φ_1 and φ_2. The fully optimized geometries for the minima, with their corresponding hydrogen-bond distances (Å) and the activation barriers, are also shown. The conformational descriptor Tn^x is also displayed. *T0* structures have a Hückel topology.

The isomerization method[19] was applied to evaluate the isomerization stabilization energies (ISEs), magnetic susceptibility exaltation[20] (Λ) and relative hardness[21] ($\Delta\eta$) of N-fused pentaphyrins **1-2**. The reactions that were used to compute the aromaticity indices of the Hückel [22]NFP and the Möbius [24]NFP are shown in Scheme 2. The *s-cis/s-trans* corrections for the isomerization stabilization energies were evaluated as the energy difference between the dihydrogen derivative of the *meso*-methyl N-fused pentaphyrin and its respective nonaromatic isomer (Figure S2).[35] The magnetic susceptibilities were computed using the CSGT method[36] at the HF/6-31+G** level of theory and the GIAO/B3LYP/6-311+G(d,p) method was used for the NICS (nucleus-independent chemical shifts) calculations.[37] NICS values were calculated at the geometrical center of the 30 heavy atoms of the pentaphyrin framework [NICS(0)] and at 1 Å above the ring center [NICS(1)]. The LUMO and HOMO energies were used for computing the hardness η of the methyl and methylene isomers involved in the isomerization method.

Ring strain was quantified using the average dihedral angle between the neighboring pyrrole rings (Φ_p). Since the evaluation of the ring strain is only based in the dihedral angles, Φ_p should be regarded as a "torsional strain" descriptor. On the other hand, the extent of effective overlap of neighboring p orbitals was measured by the torsional π-conjugation index (Π),[2] defined by Stępień as follows [Eq. (1)]:

$$\Pi = \prod_i \cos\varphi_i \qquad (1)$$

where φ_i are the dihedral angles along the classical conjugation pathway (CP). Π = 1 for a completely planar system, it is positive for any Hückel conformation and negative for any Möbius surface.

Results and discussion

Unsubstituted N-fused [22] and [24]pentaphyrins. In order to identify the most stable conformations and the interconversion pathways, we computed the potential energy surface of the N-fused [22]pentaphyin **1** at the B3LYP/6-31G(d,p) level of theory. In expanded porphyrins, the interconversion between the different π-conjugation topologies is achieved by variation of internal dihedral angles.[2] The macrocycle is preserved during the switching process, but the π system is temporarily broken when one torsion angle becomes exactly ± 90º. The surface plot of the energy versus the dihedral angles φ_1 and φ_2 from the conformation **1a** is shown in Figure 1. Three minima with a Hückel topology were located (**1a**, **1b**, **1c**) and they were fully optimized at the same level of theory.

In the discussion, the different conformations are described using the topological descriptor Tn^x, which indicates the number of half-twists (n), i.e. the linking number,[38] and the subunits located between two transoid linkages (^{X}). On the other hand, the geometrical distinction between Hückel and Möbius topology is simply assessed by counting the number of formal *trans* bonds in the smallest macrocyclic pathway (SMC).[2,39] The conformation has Möbius topology (*T1*, *T3*, etc.) when the number of *trans* bonds is odd. On the contrary, Hückel conformers contain an even number of *trans* bonds. In addition, the torsional

Journal Name RSCPublishing

ARTICLE

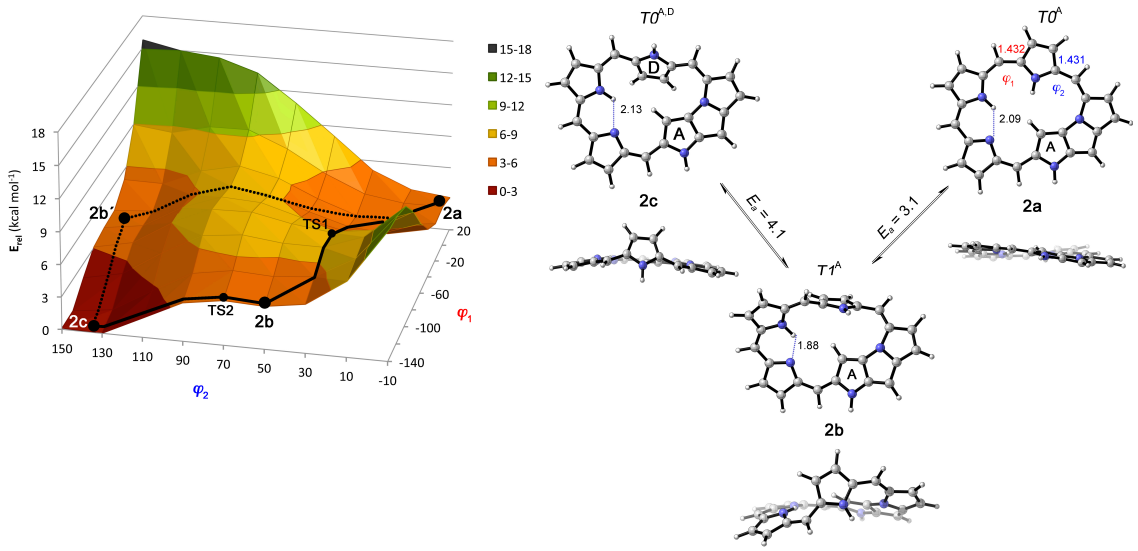

Figure 2. B3LYP/6-31G(d,p) relaxed energy potential surface for the [24]NFP **2** obtained by rotating the dihedral angles φ_1 and φ_2. The fully optimized geometries for the minima together with the activation energy barriers and the hydrogen-bond and rotating-bond distances (Å) are shown. The conformational descriptor Tn^X is also displayed. *T0* and *T1* structures have Hückel and Möbius topology, respectively.

Table 1. Relative energies (E_{rel}), topological descriptor (Tn^X) hydrogen bonding (N_H), ring strain (Φ_P), maximum deviation of dihedral angles from planarity (ψ_{MAX}), π-conjugation index (Π), and bond length alternation ($\Delta r_{C\text{-}N}$ and $\Delta r_{C\text{-}C}$) of unsubstituted [22]NFP and [24]NFP conformers.[a,b]

Conformer	Tn^X	E_{rel}	E_{rel}^D	N_H	Φ_p	ψ_{MAX}	Π	$\Delta r_{C\text{-}N}$	$\Delta r_{C\text{-}C}$
[22]NFP									
1a	$T0^A$	0.0	1.4	1	0.0	0.0	1.00	0.044	0.072
1b	$T0^{A,16}$	13.8	14.0	1	22.3	31.5	0.51	0.028	0.057
1c	$T0^{A,D}$	2.8	0.0	1	23.6	29.5	0.63	0.049	0.062
1d[c]	$T1^A$	18.2	17.8	1	35.8	82.62	-0.07	0.101	0.127
TS1$_{1a\text{-}1b}$	$T1^A$	17.3	16.4	1	36.3	62.17	-0.20	0.111	0.124
TS2$_{1b\text{-}1c}$	$T1^{A,16}$	23.2	23.1	1	36.5	74.4	-0.11	0.105	0.121
[24]NFP									
2a	$T0^A$	3.7	7.2	1	10.7	16.0	0.91	0.045	0.112
2b	$T1^A$	3.9	3.8	1	39.1	49.1	-0.26	0.019	0.083
2c	$T0^{A,D}$	0.0	0.0	1	23.6	43.1	0.52	0.044	0.107
TS1$_{2a\text{-}2b}$	$T1^A$	6.8	9.7	1	35.2	79.0	0.12	0.039	0.118
TS2$_{2b\text{-}2c}$	$T1^{A,D}$	4.1	4.8	1	38.7	69.6	-0.18	0.026	0.106

[a] E_{rel} and E_{rel}^D (in kcal mol^{-1}) were computed with the B3LYP and B3LYP-D methods, respectively. [b] Φ_p and ψ_{MAX} in deg, and $\Delta r_{C\text{-}N}$ and $\Delta r_{C\text{-}C}$ in Å. [c] **1d** is not a minimum since this geometry has one imaginary frequency.

π-conjugation index Π is positive for any Hückel (double-sided) surface and negative for any Möbius (single-sided) surface. All of these descriptors together with the relative energies of the [22]NFP conformers, computed at the B3LYP/6-31G(d,p) level of theory, are collected in Table 1. The differences in length between the shortest and longest C-C and C-N bonds (Δr) are also included in Table 1, as a measure of bond length alternation.

In absence of substituents, [22]NFP prefers the Hückel conformation **1a**, completely planar and ring-strain free (Φ_p = 0 and Π = 1). As shown in Figure 1, the low-energy pathway for the rotation of an imine-type pyrrole ring from the $T0^A$ structure **1a** involves a two-step mechanism. The conversion of **1a** to **1c** involves one intermediate conformer **1b** upon rotation of the φ_2 torsion, which is 13.8 kcal mol^{-1} less stable than **1a**. A further rotation around φ_1 in **1b** led to the D-inverted conformer **1c**, only 2.8 kcal mol^{-1} higher in energy than the totally planar conformation **1a**. In **1c**, the dihedral angles of the inverted pyrrole ring D are deviated 30º with respect to the macrocyclic plane, reducing the effective π overlap (Π = 0.63). In any case, according to the torsional π-conjugation index, **1a**, **1b** and **1c** should exhibit a distinct macrocyclic aromaticity since a Π value higher than 0.3 is expected for aromatic expanded porphyrins.

The overall activation barrier for the **1a→1c** interconversion is fairly large (E_A = 23.2 kcal mol^{-1}) and distorted Möbius topologies were found as transition states. It is remarkable that no local minima with Möbius topology were found for unsubstituted [22]NFP. The degree of bond-alternation is much larger in the Möbius transition states than that in the Hückel conformers. The large dihedral angles around the molecular twist

in both **TS1** and **TS2** preclude effective π overlap and increase the ring strain of the macrocycle. The Möbius conformation **1d** is also characterized by one imaginary frequency and it is 18.2 kcal mol^{-1} higher in energy than **1a**. The Π parameter in the Möbius transition states range form -0.07 to -0.20, suggesting that the macrocyclic conjugation is rather ineffective in these conformations. Therefore, [22]NFP strongly prefers Hückel conformations.

The relative stability of Möbius conformers is completely different for the unsubstituted [24]NFP**.** At the B3LYP/6-31G(d,p) level of theory, the Möbius conformer **2b** (with no imaginary frequencies) is only 3.9 kcal mol^{-1} higher in energy than the most stable Hückel conformation **2c**. The relaxed energy potential surface computed for **2** (Figure 2) clearly shows that the conformational flexibility is enhanced in the [24]NFP. Very low activation barriers are computed for the conformational interconversions (E_a = 3 – 4 kcal mol^{-1}), indicating that Hückel and Möbius conformers coexist in dynamic equilibrium in **2**. The overall barrier for the inversion of the pyrrole ring D in [24]NFP is only 6.8 kcal mol^{-1}, which is 16.4 kcal mol^{-1} lower than the activation barrier computed for the [22]NFP counterpart. In a previous study, the length of the rotating-bonds was directly linked to the energy barrier of the rotational process, so the longer the rotating-bond is, the lower is the rotational barrier.[40] Accordingly, the rotating-bond in **2a** is 0.036 Å larger than that of **1a**. The relative energies together with the low activation energies suggest that all the conformations are readily accessible for [24]NFP.

The relative energies computed with the empirical DFT-D dispersion correction[33] are also included in Table 1. The inclusion of the dispersion correction does not significantly affect the optimized geometries of **1a-d** and **2a-c** (Tables S1-S3). The mean absolute difference (MAD) between B3LYP and B3LYP-D conformational energies is 0.9 and 1.4 kcal mol^{-1} for **1** and **2**, respectively. The largest discrepancy between both methods corresponds to relative energy of the *T0*^{A} planar structures **1a** and **2a**, which are destabilized after the inclusion of the dispersion correction probably due to the endocyclic H···H repulsion. Consequently, the global minimum for the unsubstituted [22]NFP corresponds to the *T0*^{A,D} structure **1c** according to the B3LYP-D method. The performance of more sophisticated functionals such as M06 on the geometries and energies of *meso*-substituted will be discussed at the end.

It is noteworthy that a very similar dependence of the conformation with the oxidation state was previously found for the regular pentaphyrins. The main difference between the N-fused and non-fused pentaphyrins is the number of possible conformations. The incorporation of the N-fused moiety causes certain local conformational rigidity in the pentaphyrin macrocycle, reducing considerably the conformational freedom.

Figure 3 shows the dynamic equilibrium between two non-equivalent Möbius conformations **2b** and **2b´** and the Hückel conformer **2c** in the [24]NFP. The relative energies of the Möbius topologies **2b** and **2b´** are 3.9 and 3.2 kcal mol^{-1} respectively. The helicoidal character of both diastereomers is different (Figure 3). It is worth saying that only the conformations with a $L_K > 0$ are intrinsically chiral, having potential applications as chirality sensing and asymmetric catalysis.[38,41] The sense of chirality can be expressed by the helicity of the ribbon (*P* or *M*) or by the sign of the L_K. In Figure 3, the two enantiomers of each *T1* structures are also displayed.

According to the Π descriptor, both Möbius conformers does not exhibit a distinct macrocyclic aromaticity, as **2b** and **2b´** have Π = -0.26. The worst dihedral angle along the CP is 49º in both **2b** and **2b´**. Nevertheless, the presence of fused rings improve the macrocyclic conjugation in the Möbius conformers compared to the regular [24]pentaphyrins, since in the non-fused Möbius pentaphyrins Π = -0.17. On the contrary, the aromatic Möbius topologies of the [28]hexaphyrin and [32]heptaphyrin are characterized by fairly smooth π-conjugation surfaces with $\Pi > -0.5$. Based on the torsional descriptors, we can hypothesize that N-fused Möbius topologies show a very weak aromatic character, but still not enough to be considered as fully aromatic Möbius compounds.

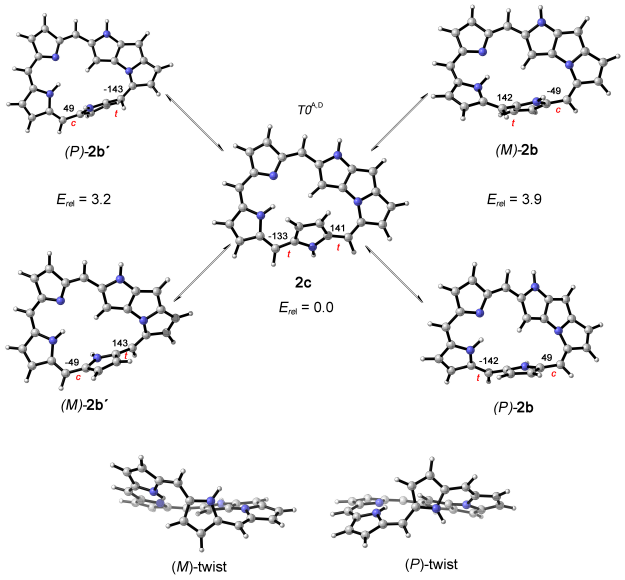

Figure 3. Conformational equilibrium of the [24]NFP **2**, switching between Hückel and Möbius topologies. **2b** and **2b´** are diastereomers and, for each *T1* structure, the two enantiomers are displayed.

In order to provide further insight into the structure-aromaticity relationship in N-fused pentaphyrins, several aromaticity descriptors based on different criteria were computed for the different conformations of **1** and **2**. The degree of aromaticity in **1a-d** and **2a-c** has been quantified using the structural (HOMA),[22] magnetic (Λ, NICS,)[20,23] energetic (ISE)[19] and reactivity ($\Delta\eta$)[21] aromaticity indices and they are collected in Table 2. The isomerization method was used to evaluate the aromatic stabilization energies (ISE), magnetic susceptibility exaltation (Λ) and relative hardness ($\Delta\eta$) of Hückel and Möbius N-fused pentaphyrins. The ISE method involves comparison of the total energies, magnetic susceptibilities and hardness of only two species: a methyl derivative of the cyclic conjugated system and its nonaromatic exocyclic methylene isomer (Scheme 2). As one closely related reference compound is involved, ISE should minimize perturbing effects such as strain. However, in previous studies, we have shown that the energetic index ISE requires the application of *s-cis*/*s-trans* correction due to unbalanced *syn-anti* diene conformations at both sides of the reaction scheme.[18,24]

Journal Name RSCPublishing

ARTICLE

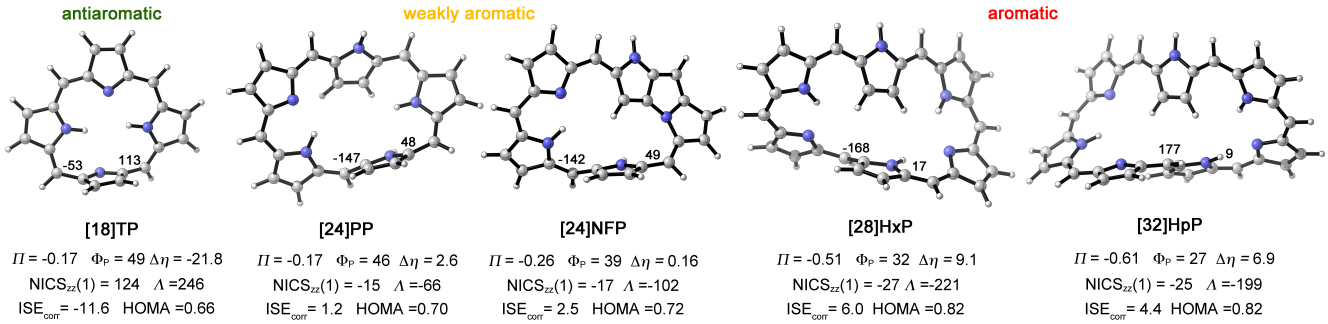

Figure 4. Möbius topologies computed for several expanded porphyrins. Dihedral angles (º) around the molecular twist, torsional descriptors and aromaticity indices are displayed.

The corrected ISE values (ISE_{corr}) are listed in Table 2. ISE_{corr} is an energetic measure of the macrocyclic aromaticity of expanded porphyrins.

Table 2. Energetic, reactivity, magnetic, and structural indices of aromaticity.[a]

Compound	ISE	ISE_{corr}	$\Delta\eta$	Λ	NICS	$NICS_{zz}(1)$	HOMA	Π
benzene	34.4	34.3	55.3	-18	-8.0	-29.2	0.982	1.00
1a (H)	26.56	5.9	3.11	-249	-16.0	-34.0	0.871	1.00
1c (H)	26.96	2.6	0.54	-190	-17.7	-30.9	0.864	0.63
1d (M)	21.57	-4.4	-3.9	-2.7	-10.0	-1.0	0.589	-0.07
2a (H)	17.85	-7.0	-13.11	410	21.9	68.4	0.670	0.91
2b (M)	18.45	2.5	0.16	-102	-12.0	-16.9	0.720	-0.26
2c (H)	22.2	-4.9	-9.37	204	6.6	38.0	0.622	0.52

[a] ISE_{corr} and $\Delta\eta$ are given in kcal mol^{-1}, Λ in ppm cgs and NICS indices in ppm.

A close relationship between the molecular topology, the number of π-electrons in the CP and the macrocyclic aromaticity exists. In agreement with the annulene model, all the Hückel conformations with [22] π-electrons (**1a-1c**) are highly aromatic, with positive ISE_{corr} and $\Delta\eta$ values, highly negative Λ and NICS values as well as a bond-delocalized structure. The inversion of the D-pyrrole ring in **1c** reduces the macrocyclic aromaticity relative to the completely planar conformation **1a**. On the contrary, the Hückel conformations of [24]NFP are antiaromatic since they are energetically destabilized and exhibit bond-localized structures and strong paramagnetic ring currents. The antiaromaticity of **2c** is weaker than that of **2a** as a consequence of the loss of planarity. Consistent with the concept of the Möbius aromaticity, the sign of the aromaticity descriptors is reverse for Möbius conformations **1d** and **2b**. The magnetic properties of **2b** support weak diatropic ring currents, although the degree of aromaticity of the Möbius topology is significantly lower than the aromaticity of the Hückel conformations of the [22]NFP.

In order to characterize the minimum size of expanded porphyrins that can achieve Möbius aromaticity, we compare the aromaticity descriptors of several Möbius expanded porphyrins. Figure 4 displays the Möbius conformers of the porphyrin ([18]TP), N-fused and regular pentaphyrins ([24]NFP and [24]PP), hexaphyrin ([28]HxP) and protonated heptaphyrin ([32]HpP), together with their torsional descriptors and aromaticity indices. According to the ring strain descriptor Φ_p, the torsional strain of the Möbius topology is conveniently reduced by increasing the size of the macrocycle. On one hand, the tetrapyrrolic porphyrin skeleton is not large enough to implement Möbius twisted topology. The Möbius conformer of the regular porphyrin is a transition state and it is predicted to be 63 kcal mol^{-1} higher in energy than the planar conformer. The molecular twist significantly increases the ring strain of the [18]annulenoid system and the π-conjugation is rather inefficient (Π = -0.17). On the other hand, the overlap of the π-orbitals is quite effective in the Möbius topologies of [28]hexaphyrin and protonated [32]heptaphyrin, resulting in a distinct macrocyclic aromaticity. In the Möbius structures of [24]PP and [24]NFP, the Π values are small and they are less aromatic than the larger Möbius topologies according to all the aromaticity descriptors. The structural, magnetic, energetic and reactivity descriptors suggest that the degree of macrocyclic aromaticity for the Möbius topologies decreases in the order: [28]HxP ≥ [32]HpP > [24]NFP > [24]PP. Except the relative hardness, the aromaticity indices confirm that the N-fused pentaphyrins exhibit higher macrocyclic aromaticity than the regular [24]PP. In any case, it seems that the planarity enforced by Rh(I) metalation is important for the manifestation of a distinct macrocyclic aromaticity in this compound.[28]

The statistical analysis revealed significant correlations among the various aromaticity criteria, so the energetic, magnetic, structural and reactivity descriptors distinguish between aromatic and antiaromatic N-fused pentaphyrins in a roughly similar way. Thus, all conformers with diatropic and paratropic ring currents

have positive and negative ISE_{corr} and $\Delta\eta$, respectively. As we observed previously for several expanded porphyrins,[18,25] excellent correlations exist between all the magnetic descriptors (Table S4). The isomerization method provides exaltation values Λ strongly correlated with the NICS-based descriptors, specially the out-of-plane component $NICS_{zz}(1)$ (R^2 = 0.995 Figure 5a). However, it should be noted that Λ and, to a lesser extent NICS, are dependent on the square of the ring area and, consequently all magnetic descriptors point out that the effect of aromaticity is higher in N-fused pentaphyrins than in benzene. On the contrary, the energetic, reactivity and structural indices point out that the effect of aromaticity is much smaller in such large macrocycles than in benzene.

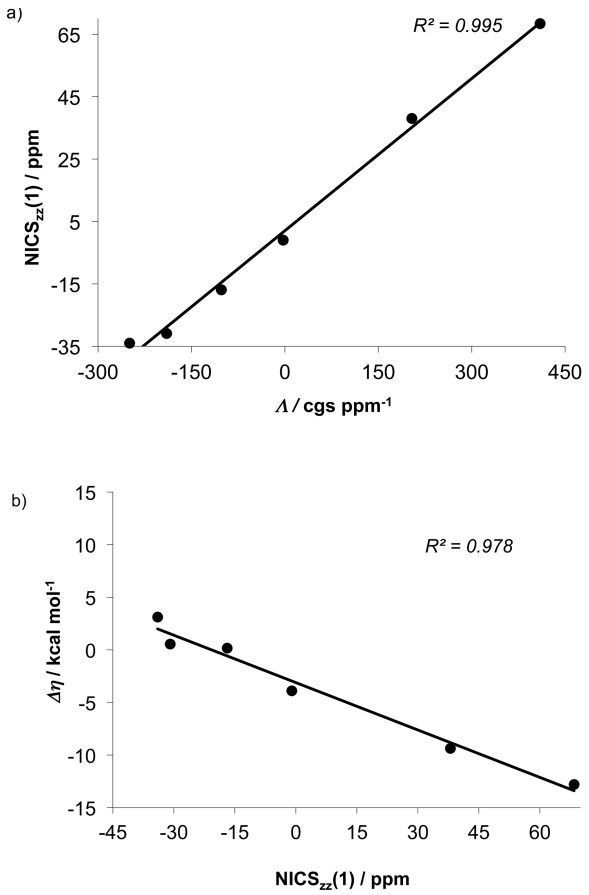

Figure 5. Correlation between the magnetic susceptibility exaltation (Λ) and the relative hardness ($\Delta\eta$) with the out-of-plane component of the NICS tensor computed at 1 Å [$NICS_{zz}(1)$] for the studied N-fused pentaphyrins.

Interestingly, the relative hardness ($\Delta\eta$) is very well correlated with the magnetic descriptors (R^2 = 0.978, Figure 5b). This conceptual DFT based descriptor is not size-dependent and, therefore, it can be applied to different-sized compounds. The correlation with the corrected energetic descriptor ISE_{corr} is worse, although still R^2 = 0.890. It is remarkable that the correlations of the energetic descriptor with the rest of the aromaticity indices improve significantly after the application of the *s-cis*/*s-trans* corrections (Figure S1). Regardless of the number of π electrons and the molecular topology, the uncorrected ISE values are positive for all the conformations of the N-fused pentaphyrins.

The worst correlations are found for the structural aromaticity index HOMA. HOMA predicts correctly that the Hückel conformers are more aromatic than the Möbius structures for the [22]NFP and *viceversa* for the [24]NFP. However, the Hückel conformers of **2** that exhibit a larger bond equalization (**2a**) have stronger paratropic ring currents and thus more antiaromatic magnetic properties. In addition, the differences in the HOMA values between the weakly aromatic Möbius conformer **2b** and the antiaromatic Hückel conformers (**2a** and **2c**) are very small. Accordingly, the widely used HOMA index should be used with caution in evaluating the macrocyclic aromaticity of expanded porphyrins.[42] On the basis of our results, the use of the magnetic and reactivity indices to quantify the aromaticity/antiaromaticity of expanded porphyrins is strongly recommended.

Substituent effect on the conformation of N-fused pentaphyrins. A very effective way for tuning the conformations of expanded porphyrins is by modification of the substituents at the *meso* carbons.[1,43] Previously, we have demonstrated that conformational control of pentaphyrins can be achieved by changing the number of *meso*-substituents.[25] The removal of one aryl group prevents the N-fusion reaction, providing stable aromatic non-fused [22]pentaphyrins adopting a $T0^{4,D}$ conformation. Herein, we have investigated the influence of the nature of the *meso*-substituent on the conformation of N-fused pentaphyrins at both oxidation states. To this end, we have chosen several substituents (CH_3, CF_3, C_6F_5, 2,6-Cl_2-phenyl), commonly used in the synthesis of expanded porphyrins. Experimental information on the conformations of these *meso*-substituted N-fused pentaphyrins is currently available, being certainly appropriate to test our computational results.

Table 3. Relative energies (in kcal mol^{-1}) of *meso*-substituted N-fused pentaphyrins.

Label	**1**	**3**	**5**	**7**	**9**
[22]NFP	H	CH_3	CF_3	C_6F_5	$C_6H_3Cl_2$
$T0^{A}$	0.0	$T1^{A}$	$T1^{A}$	9.6	11.9
$T0^{A,D}$	2.8	0.0	0.0	0.0	0.0
$T1^{A}$	18.2[a]	9.6	2.5	4.0	$T0^{A,D}$
Label	**2**	**4**	**6**	**8**	**10**
[24]NFP	H	CH_3	CF_3	C_6F_5	$C_6H_3Cl_2$
$T0^{A}$	3.7	$T1^{A}$	$T1^{A}$	$T1^{A}$	$T1^{A}$
$T0^{A,D}$	0.0	1.9	4.4	1.2	0.0
$T1^{A}$	3.9	0.0	0.0	0.0	1.5

[a] The Möbius topology $T1^{A}$ of compound **1** is a transition state.

The relative energies of the different conformations computed at the B3LYP/6-31G(d,p) level of theory are collected in Table 3. The optimized geometries of the global minimum of the respective meso-substituted N-fused pentaphyrins are shown in Figure 6. For both oxidation levels, the $T0^{A}$ conformation is highly destabilized by *meso*-substituents. In most of the cases, the optimization of the $T0^{A}$ conformation with five *meso*-substituents led to a Möbius structure ($T1^{A}$).

Journal Name RSCPublishing

ARTICLE

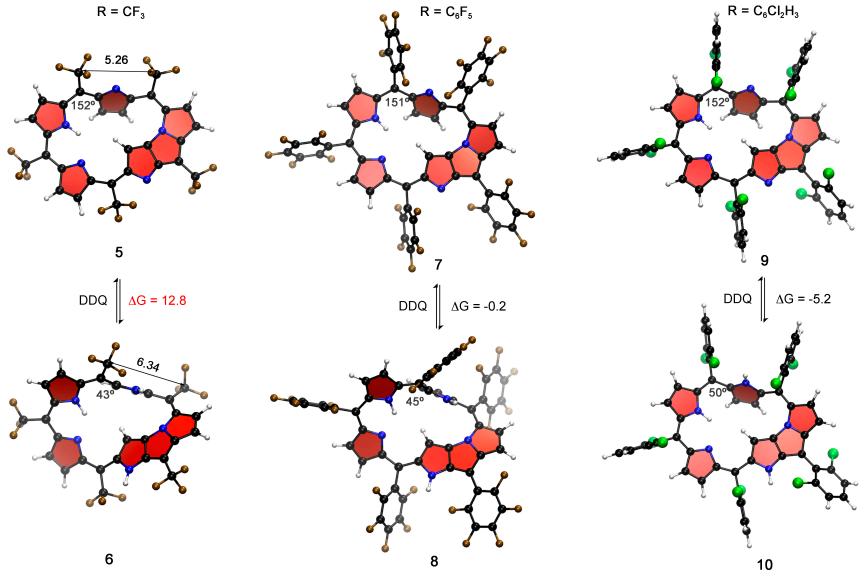

Figure 6. The most stable conformations of *meso*-substituted N-fused [22] and [24]pentaphyrins at the B3LYP/6-31G(d,p) level of theory . The most distorted dihedral angle from planarity along the conjugation pathway is also indicated. Gibbs free energies (in kcal mol^{-1}) for the oxidation reaction [24]NFP→[22]NFP are also shown.

With 22π-electrons, the $T0^{A,D}$ conformation is preferred for all the substituents. As shown by the torsional descriptors in Table 4, this conformation shows smaller deviations from planarity along the CP and consequently more effective overall conjugation than the other conformers. A large negative NICS value calculated at the geometrical center of the macrocycle supports a high aromatic character of this structure (-16.4 ppm in **7** and -16.7 ppm in **9**). In good agreement with the theoretical results, the X-ray diffraction analysis revealed a $T0^{A,D}$ conformation for the *meso*-(2,6-dichlorophenyl) [22]NFP (**9**).[27] Moreover, the ^{1}H NMR spectra indicate the **7** and **9** possess a distinct diatropic ring current as revealed by the chemical shifts of the inner C-H and N-H protons.[28] In the case of the CF_3 group, it was not possible experimentally to isolate the [22]NFP counterpart.[44] A remarkable characteristic of *meso*-substituted **[**22]NFP is that distorted Möbius conformations are local minima on the PES with all real vibrational frequencies. However, they are higher in energy than the Hückel topology $T0^{A,D}$ and the π-conjugation is rather inefficient (Table 4).

In the case of the [24]NFP, the conformation of the macrocycle depends on *meso*-substituents. Whereas the (2,6)-dichlorophenyl groups prefers a Hückel $T0^{A,D}$ conformation, the CF_3 and C_6F_5 substituents prefer a Möbius $T1^A$ conformation. In good agreement with the relative energies predicted by B3LYP, the solid-state structure of **10** corresponds to the Hückel $T0^{A,D}$ conformation, whereas a Möbius topology was found in the crystal structure of **6** and **8**.[28,44] Nevertheless, considering the small energy differences between the $T0^{A,D}$ and $T1^A$ conformers as well as the small activation energy barriers computed for **2**, we anticipate that N-fused [24]pentaphyrins exist in solution as an equilibrium of Hückel and Möbius conformers. In fact, the ^{1}H NMR spectra of the **6**, **8** and **10** show characteristics of moderate paratropicity, suggesting a plausible equilibrium between *T0* and *T1* conformers. The difference between the most upfield and the most downfield chemical shifts for the *β*-CH signals are -7.42 ppm for **10** and -2.60 for **8**, indicating a stronger paratropic ring current in **10.**[28]

Table 4. Maximum deviation of dihedral angles from planarity (ψ_{MAX}), π-conjugation index (*Π*) and HOMA of *meso*-substituted N-fused pentaphyrins.

R	Tn^X	ψ_{MAX}	*Π*	HOMA	R	Tn^X	ψ_{MAX}	*Π*	HOMA
	[22]NFP					**[24]NFP**			
CF_3	$T0^{A,D}$	28.4	0.64	0.840	CF_3	$T0^{A,D}$	73.4	0.17	0.510
	$T1^A$	57.0	-0.25	0.524		$T1^A$	43.2	-0.25	0.668
	$T0^A$	55.2	0.33	0.752					
C_6F_5	$T0^{A,D}$	28.3	0.64	0.719	C_6F_5	$T0^{A,D}$	51.4	0.45	0.58
	$T1^A$	57.0	-0.27	0.567		$T1^A$	45.0	-0.27	0.73
$C_6H_3Cl_2$	$T0^{A,D}$	29.4	0.64	0.725	$C_6H_3Cl_2$	$T0^{A,D}$	50.0	0.46	0.586
	$T0^A$	52.5	0.35	0.680		$T1^A$	43.6	-0.28	0.75

According to the relative energies, this conformational equilibrium can be controlled by *meso*-substituents. On one hand, the contribution of the Hückel antiaromatic conformation

should be particularly important in **10**, explaining the larger paratropic ring current observed for this compound. On the other hand, the *T1* conformer should prevail in the conformational equilibrium of **6**, explaining the diatropic shielding of the inner β-CH proton of pyrrole ring A whose signal appears as 3.09 ppm.[44] A weak diatropic ring current is supported by the NICS value of the Möbius conformation of **6** (-10.5 ppm). Again, the low absolute values of Π suggest that the macrocyclic conjugation is still ineffective in these *T1* conformations for displaying a distinct Möbius aromaticity.

The Gibbs free energies (ΔG_{298}) computed for the oxidation reaction of the [24]NFP→[22]NFP are also displayed in Figure 6. 2,3-dichloro-5,6-dicyano-1,4-benzoquinone (DDQ) was used as oxidant, being reduced to the corresponding hydroquinone ($DDQH_2$). In the case of *meso*-aryl-substituted pentaphyrins (**8** and **10**), the thermodynamic data support that reversible redox interconversions between [24] and [22]NFP are feasible in agreement with the experimental observations. Accordingly, both oxidation states are stable for the pentafluorophenyl and (2,6)-dichlorophenyl substituents. On the contrary, the oxidation of the [24]NFP **6** to its **5** counterpart is not thermodynamically allowed with the CF_3 groups, as revealed by the ΔG_{298} = 12.8 kcal mol^{-1}. In good agreement with the theoretical results, the oxidation of **6** to its [22]NFP was found to be difficult even with DDQ or MnO_2 under forcing conditions.[44] The instability of the Hückel [22]NFP seems to be related with the steric hindrance between the bulky CF_3 groups. Whereas in the Möbius [24]NFP the *meso*-substituents adjacent to the tilted pyrrole ring D are in *trans,* separated by 6.33 Å; in the Hückel [22]NFP they are in *cis* with a relative distance of 5.26 Å (Figure 6).

DFT benchmark study for Möbius and Hückel N-fused pentaphyrins. The modest computational cost of DFT makes it the best method to study large expanded porphyrins. The performance of the three-parameter hybrid functional B3LYP on the geometries of N-fused pentaphyrins has been assessed using the X-ray structures as a reference. Recently, it has been shown that B3LYP could give rise to large errors in the relative energy of several conjugated systems.[45] In addition, conventional functionals are not able to account for the nonbonding interactions accurately due mainly to the lack of medium- and long-range dispersion.[33b,46] Accordingly, new density functionals such as M06 and also *posteriori* corrections for existing functionals has been recently proposed. Therefore, we also performed the calculations on *meso*-substituted N-fused pentaphyrins with both M06 functional[34] and the DFT-D semi-empirical dispersion correction.[33]

The performance of the different DFT methods in reproducing the molecular structure of several N-fused pentaphyrins (**6** and **8-10**) was first assessed by comparison with the X-ray diffraction data (Figure 7). Several statistical criteria were considered in our benchmark study: the root-mean-square deviation (RMSD) between the DFT-optimized and X-ray sets of Cartesian coordinates and the mean absolute error (MAE) from comparison of selected interatomic distances and dihedral angles. Table 5 contains the RMSD for the superimposed structures considering the geometry of the macrocycle alone ($RMSD_{30}$) and the all-heavy-atoms ($RMSD_{heavy}$), the MAE for the bond lengths and dihedral angles along the classical conjugation pathway and the torsional descriptors.

Table 5. Root-mean-square deviations (RMSD in Å) and mean absolute errors (MAE) of the DFT optimized geometries relative to the X-ray structures of N-fused pentaphyrins together with the torsional descriptors (ψ_{MAX} and Π) and the HOMA values.

	$RMSD_{30}$	$RMSD_{heavy}$	MAE_{bonds}	$MAE_{torsions}$	HOMA	ψ_{MAX}	Π
[22]NFP **9**			$C_6H_3Cl_2$	Hückel			
RX	0.00	0.00	0.000	0.0	0.803	29.3	0.673
B3LYP	0.10	0.33	0.016	2.4	0.840	28.4	0.640
B3LYP-D	0.10	0.34	0.015	2.3	0.864	27.3	0.654
M06	0.09	0.43	0.019	2.5	0.833	31.3	0.632
[24]NFP **8**			C_6F_5	Möbius			
RX	0.00	0.00	0.000	0.0	0.565	59.0	-0.208
B3LYP	0.21	0.90	0.016	4.4	0.732	45.0	-0.272
B3LYP-D	0.24	0.91	0.015	4.3	0.752	44.5	-0.269
M06	0.21	0.78	0.012	4.2	0.761	48.1	-0.254
[24]NFP **6**			CF_3	Möbius			
RX	0.00	0.00	0.000	0.0	0.586	64.0	-0.166
B3LYP	0.17	0.43	0.014	4.114	0.687	42.8	-0.266
B3LYP-D	0.20	0.44	0.016	4.798	0.725	40.3	-0.265
M06	0.17	0.36	0.010	3.903	0.721	44.1	-0.256
[24]NFP **10**			$C_6H_3Cl_2$	Hückel			
RX	0.00	0.00	0.000	0.0	0.398	63.08	0.398
B3LYP	0.09	0.31	0.019	3.9	0.586	49.98	0.586
B3LYP-D	0.11	0.29	0.019	4.1	0.631	44.23	0.631
M06	0.07	0.30	0.016	3.8	0.644	50.82	0.644

For the *meso*-(2,6-dichlorophenyl)-substituted [22]NFP **9**, the B3LYP-optimized geometry are in better agreement with the X-ray structure when considering the overall structure. However, for the Möbius [24]NFP **8** and **6** the lowest RMSD corresponds to the M06-optimized geometries. In the case of the Hückel [24]NFP **10**, B3LYP-D gave the lowest RMSD. The best overall performance is observed for M06, which offer the smallest MAE in most of the cases when considering the selected geometrical parameters. However, the degree of bond alternations of the crystallographic structures of N-fused pentaphyrins is better reproduced by the B3LYP functional, as can be inferred from the HOMA values. In any case, the optimized geometries obtained with B3LYP and M06 are very similar according to the RMSD and MAE values. Moreover, a better description of the macrocycle is achieved for the Hückel structures **9** and **10** as compared with the Möbius topologies. The $RMSD_{30}$ increases considerably for the Möbius structures **6** and **8**, and the maximum differences between the experimental and calculated values correspond to the dihedral angles around the molecular twist.

Table 6 is used to examine the performance of the different methods on the relative energies of the different conformers of the N-fused [24] and [22]pentaphyrins. All the methods yield the same energy ordering of the conformers of the *meso*-substituted N-fused pentaphyrins. All the methods predict the Hückel conformation $T0^{A,D}$ as most stable for [22]NFP bearing aryl

Journal Name RSCPublishing

ARTICLE

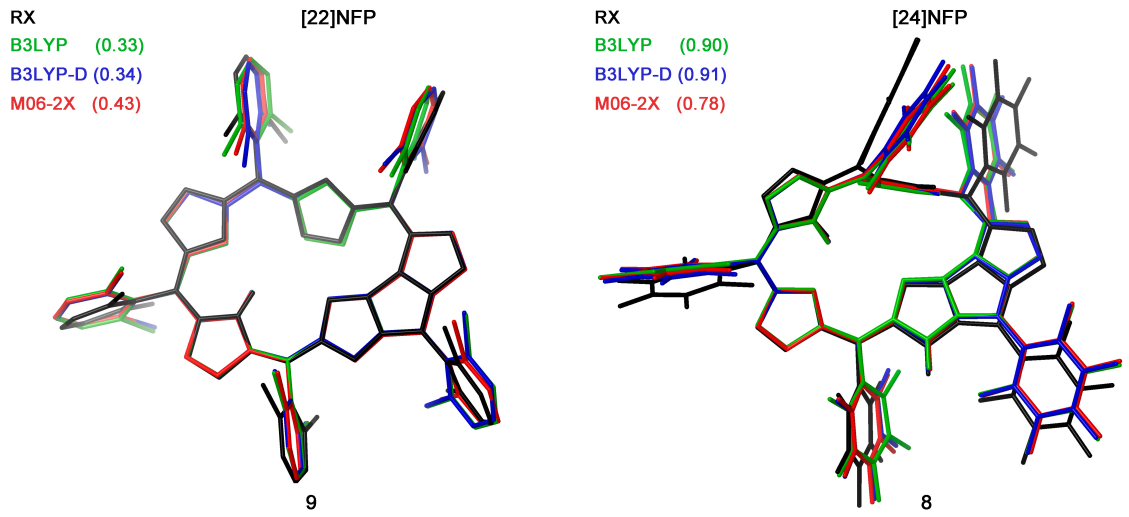

Figure 7. Comparison of B3LYP, B3LYP-D and M06-2X optimized geometries of N-fused pentaphyrins, overlaid with the X-ray structure of **9** and **8**. The all-heavy-atom RMSDs (in Å) are in parenthesis.

groups. In the case of the [24]NFP, all the methods point out that the Hückel $T0^{A,D}$ conformation is the global minima for the $C_6H_3Cl_2$ substituent, whereas the Möbius topology is the most stable conformation for the CF_3 and C_6F_5 substituents.

Table 6. Relative energies (in kcal mol^{-1}) of *meso*-substituted N-fused pentaphyrins computed with different DFT methods.

Label	CF_3 (**5**)		C_6F_5 (**7**)		$C_6H_3Cl_2$ (**9**)	
[22]NFP	$T1^A$	$T0^{A,D}$	$T0^A$	$T0^{A,D}$	$T0^A$	$T0^{A,D}$
B3LYP	2.5	0.0	9.6	0.0	11.9	0.0
B3LYP-D	3.2	0.0	12.3	0.0	12.6	0.0
M06	3.0	0.0	11.3	0.0	11.9	0.0
Label	CF_3 (**6**)		C_6F_5 (**8**)		$C_6H_3Cl_2$ (**10**)	
[24]NFP	$T1^A$	$T0^{A,D}$	$T1^A$	$T0^{A,D}$	$T1^A$	$T0^{A,D}$
B3LYP	0.0	4.4	0.0	1.5	1.2	0.0
B3LYP-D	0.0	5.2	0.0	1.2	0.2	0.0
M06	0.0	4.0	0.0	1.2	2.0	0.0

Importantly, there are no significant differences in the conformational relative energies computed with the different methods with a MAE of 0.5 kcal mol^{-1} (for B3LYP-D) and 0.3 kcal mol^{-1} (for M06). It is important to stress that a large influence of the computational method on the conformational energies was previously observed in *meso*-substituted [32]heptaphyrins.[24] In this expanded porphyrin, we found that the attractive π-π stacking interactions in the figure-eight conformation are overemphasized in the dispersion-corrected methods and only B3LYP provided relative energies in full agreement with the experimental evidence. In the case of the N-fused pentaphyrins, B3LYP and M06 show the best overall performance for describing the geometries and both methods yielded very similar energies. Remarkably, our computational results support all the experimental data available for N-fused pentaphyrins.

Conclusions

The conformational preferences, interconversion pathways and aromaticity of N-fused [22] and [24]pentaphyrins have been investigated using density functional theory calculations. The conformation of the macrocycle is shown to be strongly dependent on the oxidation state, aromaticity of the π-electron system and *meso*-substituents.

Whereas N-fused [22]pentaphyrins strongly prefers a Hückel conformation $T0^{A,D}$, Hückel and Möbius conformers coexist in dynamic equilibrium for the [24] congener. The Hückel-Möbius aromaticity switch requires very low activation energy barrier (E_a = 3-4 kcal mol^{-1}). Interestingly, the balance between $T0^{A,D}$ and $T1^A$ conformations in [24]NFP can be controlled by *meso*-substituents. Conversely, the inversion of a pyrrole ring in the [22]NFP occurs via Möbius transition structures and requires relatively high activation energy barriers (E_a = 23 kcal mol^{-1}). The N-fused moiety reduces considerably the conformational

freedom of the macrocycle compared to the regular non-fused pentaphyrins, influencing the conformational balance.

The energetic, magnetic, reactivity and structural aromaticity indices reveal a close relationship between the molecular topology, the number of π-electrons and aromaticity. Hückel conformations with [22] π-electrons are strongly aromatic, whereas Hückel structures with [24] π-electrons are antiaromatic. The Möbius structures of [24]NFP exhibit a very weak aromatic character due to the large dihedral angles around the molecular twist, being significantly less aromatic than the Möbius topologies of [28]hexaphyrin and [32]heptaphyrin. The aromaticity of N-fused pentaphyrins is revealed best by the magnetic indices and the relative hardness rather than the structural and energetic descriptors.

Regarding to the computational methodology, we show that M06 and B3LYP predicts geometries for both Möbius and Hückel conformations of *meso*-substituted N-fused pentaphyrins in better agreement with experiment than B3LYP-D. Nevertheless, there are not significant differences between the conformational relative energies computed with the different functionals. Our computational results support the experimental evidence available for N-fused pentaphyrins and therefore, it is shown that density functional theory calculations are a powerful tool in aiding the design of *viable* Möbius aromatic expanded porphyrins.

Acknowledgements

M. A. thanks the European Community for financial support through the postdoctoral fellowship FP7-PEOPLE-2010-IEF-273527. P. G. and F. D. P wishes to thank the Fund for Scientific Research–Flanders (FWO) and the Free University of Brussels (VUB) for their continuous support and the VUB Strategic Research Program of ALGC in the context of which these investigations were carried out.

Notes and references

[a] Eenheid Algemene Chemie (ALGC), Vrije Universiteit Brussel (VUB), Pleinlaan 2, 1050 Brussels (Belgium).

Electronic Supplementary Information (ESI) available: relationships between aromaticity indices, *syn-anti* corrections for the isomerization stabilization energies; B3LYP-6-31G(d,p)-optimized geometries. See DOI: 10.1039/b000000x/

1 S. Saito and A. Osuka, *Angew. Chem. Int. Ed.*, 2011, **50**, 4342.

2 M. Stępień, N. Sprutta and L. Latos-Grażyński, *Angew. Chem. Int. Ed.*, 2011, **50,** 4288.

3 B. M. Rambo and J. L. Sessler, *Chem. Eur. J.*, 2011, **17**, 4946.

4 (*a*) Y. Ikawa, M. Takeda, M. Suzuki, A. Osuka and H. Furuta, *Chem. Commun.* 2010, **46**, 5689; (*b*) A. Osuka, T. Tanaka and H. Mori, *J. Mat. Chem. C* 2013, **1**, 2500.

5 (*a*) M. O. Senge, M. Fazekas, E. G. A. Notaras, W. J. Blau, M. Zawadzka, O. B. Locos and E. M. Ni Mhuircheartaigh, *Adv. Mater.*, 2007, **19**, 2737; (*b*) M. Pawlicki, H. A. Collins, R. G. Denning and H. L. Anderson, *Angew. Chem. Int. Ed.*, 2009, **48**, 3244.

6 (*a*) J. M. Lim, Z. S. Yoon, J. Y. Shin, K. S. Kim, M. C. Yoon and D. Kim, *Chem. Commun.*, 2009, 261; (*b*) M. C. Yoon, S. Cho, M. Suzuki, A. Osuka and D. Kim, *J. Am. Chem. Soc.*, 2009, **131**, 7360.

7 A. Osuka and S. Saito, *Chem. Commun.*, 2011, **47**, 4330.

8 E. Heilbronner, *Tetrahedron Lett*., 1964, **5**, 1923.

9 D. Ajami, O. Oeckler, A. Simon and R. Herges, *Nature*, 2003, **426**, 819

10 J. Y. Shin, K. S. Kim, M. C. Yoon, J. M. Lim, Z. S. Yoon, A. Osuka and D. Kim, *Chem. Soc. Rev,*, 2010, **39**, 2751.

11 M. Torrent-Sucarrat, J. M. Anglada and J. M. Luis, *J. Chem. Phys.*, 2012, **137**, 184306.

12 (*a*) Z. S. Yoon, D.-G. Cho, K. S. Kim, J. L. Sessler and D. Kim, *J. Am. Chem. Soc.*, 2008, **130**, 6930; (*b*) S. Mori, K. S. Kim, Z. S. Yoon, S. B. Noh, D. Kim and A. Osuka, *J. Am. Chem. Soc.* 2006, **129**, 11344; (*c*) M.-C. Yoon, S. Cho, M. Suzuki, A. Osuka and D. Kim, *J. Am. Chem. Soc.*, 2009, **131**, 7360.

13 Z. S. Yoon,, J. H. Kwon, M.-C. Yoon, M. K. Koh, S. B. Noh,, J. L. Sessler, J. T. Lee, D. Seidel, A. Aguilar, S. Shimizu, M. Suzuki, A. Osuka, and D. Kim, *J. Am. Chem. Soc.*, 2006, **128**, 14128;

14 F. Sondheimer, R. Wolovsky and Y. Amiel, *J. Am. Chem. Soc.*, 1962, **84**, 274.

15 In both Hückel and Möbius all-pyrrole porphyrinoids, the annulene-like conjugation pathway (CP) passes through the iminic nitrogens and circumvents the amino NH groups.

16 (*a*) A. R. Katritzky, K. Jug and D. C. Oniciu, *Chem. Rev*., 2001, **101**, 1421; (*b*) M. Alonso and B. Herradón, *Phys. Chem. Chem. Phys*., 2010, **12**, 1305.

17 J. I. Wu, I. Fernández and P. v. R. Schleyer, *J. Am. Chem. Soc*., 2012, **135**, 315.

18 M. Alonso, P. Geerlings and F. De Proft, *Chem. Eur. J*., 2012, **18**, 10916.

19 P. v. R. Schleyer and F. Pühlhofer, *Org. Lett.*, 2002, **4**, 2873.

20 H. J. Dauben, J. D. Wilson and J. L. Layti, *J. Am. Chem. Soc.*, 1968, **90**, 811.

21 F. De Proft and P. Geerlings, *Phys. Chem. Chem. Phys.* 2004, **6**, 242.

22 (*a*) J. Kruszewski and T. M. Krygowski, *Tetrahedron Lett*., 1972, **13**, 3839; (*b*) T. M. Krygowski, *J. Chem. Inf. Comput. Sci*., 1993, **33**, 70.

23 (*a*) P. v. R. Schleyer, C. Maerker, A. Dransfeld, H. J. Jiao and N. Hommes, *J. Am. Chem. Soc.* 1996, **118**, 6317; (*b*) Z. Chen, C. S. Wannere, C. Corminboeuf, R. Puchta and P. v. R. Schleyer, *Chem. Rev.,* 2005, **105**, 3842.

24 M. Alonso, P. Geerlings and F. De Proft, *Chem. Eur. J*., 2013, **19**, 1617.

25 M. Alonso, P. Geerlings and F. De Proft, *J. Org. Chem*., 2013, **78**, 4419.

26 J.-Y. Shin, H. Furuta and A. Osuka, *Angew. Chem. Int. Ed*., 2001, **40**, 619.

27 S. Mori, J.-Y. Shin, S. Shimizu, F. Ishikawa, H. Furuta and A. Osuka, *Chem. Eur. J*., 2005, **11**, 2417.

28 J. K Park, Z. S. Yoon, M.-C. Yoon, K. S. Kim, S. Mori, J.-Y. Shin, A. Osuka and D. Kim, *J. Am. Chem. Soc*., 2008**, 130**, 1824.

29 T. Higashino and A. Osuka, *Chem. Sci.*, 2012, **3**, 103.

30 M. J. Frisch, G. W. Trucks, H. B. Schlegel, G. E. Scuseria, M. A. Robb, J. R. Cheeseman, G. Scalmani, V. Barone, B. Mennucci, G. A. Petersson, H. Nakatsuji, M. Caricato, X. Li, H. P. Hratchian, A. F. Izmaylov, J. Bloino, G. Zheng, J. L. Sonnenberg, M. Hada, M. Ehara, K. Toyota, R. Fukuda, J. Hasegawa, M. Ishida, T. Nakajima, Y. Honda, O. Kitao, H. Nakai, T. Vreven, J. A. Montgomery, Jr., J. E. Peralta, F.

Ogliaro, M. Bearpark, J. J. Heyd, E. Brothers, K. N. Kudin, V. N. Staroverov, T. Keith, R. Kobayashi, J. Normand, K. Raghavachari, A. Rendell, J. C. Burant, S. S. Iyengar, J. Tomasi, M. Cossi, N. Rega, J. M. Millam, M. Klene, J. E. Knox, J. B. Cross, V. Bakken, C. Adamo, J. Jaramillo, R. Gomperts, R. E. Stratmann, O. Yazyev, A. J. Austin, R. Cammi, C. Pomelli, J. W. Ochterski, R. L. Martin, K. Morokuma, V. G. Zakrzewski, G. A. Voth, P. Salvador, J. J. Dannenberg, S. Dapprich, A. D. Daniels, O. Farkas, J. B. Foresman, J. V. Ortiz, J. Cioslowski and D. J. Fox, *Gaussian 09*, *Revision B.01*, Gaussian, Inc., Wallingford CT, 2010.

31 A. D. Becke, J. Chem. Phys. 1993, 98, 5648.

32 For a detailed account on these types of basis sets, see e.g. W. J. Hehre, L. Radom, P. v. R. Schleyer and J. A. Pople, Ab Initio Molecular Orbital Theory, Wiley, New York, 1986.

33 (*a*) S. Grimme, *J. Comput. Chem.* 2004, **25**, 1463S; (*b*) Ehrlich, J. Moellmann and S. Grimme, *Acc. Chem. Res.*, 2012, **46**, 916.

34 Y. Zhao and D. G. Truhlar, *Theor. Chem. Acc.*, 2008, **120**, 215.

35 C. S. Wannere, D. Moran, N. L. Allinger, Hess, B. Andes, L. J. Schaad and P. v. R. Schleyer, *Org. Lett.*, 2003, **5**, 2983.

36 T. A. Keith; R. F. W. Bader, *Chem. Phys. Lett.*, 1993, **210**, 223.

37 K. Wolinski, J. F. Hinton and P. Pulay, *J. Am. Chem. Soc.*, 1990, **112**, 8251.

38 S. M. Rappaport and H. S. Rzepa, *J. Am. Chem. Soc.*, 2008, **130**, 7613.

39 R. Herges, *Chem. Rev.* 2006, **106**, 4820.

40 E. Marcos, J. M. Anglada and M. Torrent-Sucarrat, *J. Phys. Chem. C*, 2012, **116**, 24358.

41 T. Tanaka, T. Sugita, S. Tokuji, S. Saito and A. Osuka, *Angew. Chem. Int. Ed.*, 2010, **49**, 6619.

42 A similar conclusion was drawn by: H. Fliegl, D. Sundholm, S. Taubert and F. Pichierri, *J. Phys. Chem. A.*, 2010, **114**, 7153.

43 (*a*) M. Suzuki and A. Osuka, *Chem. Eur. J.*, 2007, **13**, 196; (*b*) S. Saito, J. Y. Shin, J. M. Lim, K. S. Kim, D. Kim and A. Osuka, *Angew. Chem. Int. Ed.*, 2008, **47**, 9657.

44 S. Shimizu, N. Aratani and A. Osuka, *Chem. Eur. J.*, 2006, **12,** 4909.

45 (*a*) P. R. Schreiner, *Angew. Chem. Int. Ed.*, 2007, **46**, 4217; (*b*) P. Mori-Sanchez, A. J. Cohen and W. Yang, *J. Chem. Phys.*, 2006, **125**, 201102; (*c*) M. D. Wodrich, C. Corminboeuf and P. v. R. Schleyer, *Org. Lett.*, 2006, **8**, 3631.

46 (*a*) K. E. Riley, M. Pitoňák, P. Jurečka and P. Hobza, *Chem. Rev.*, 2010, **110**, 5023; (*b*) E. G. Hohenstein and C. D. Sherrill, *WIREs. Comput. Mol. Sci.*, 2012, **2**, 304.